International Journal of Thermophysics, Vol. 3, No. 4, 1982

Experimental and Theoretical Studies of the Influence of Surface Conditions on Radiative Properties of Opaque Materials

P. Demont,[1] M. Huetz-Aubert,[1] and H. Tran N'Guyen[1]

Received May 4, 1982

Radiative properties of opaque materials strongly depend on their surface condition. The fabrication of superficial cavities of various forms and dimensions modifies the directional spectral emissivities or absorptivities. They are usually increased compared to those of optically smooth material; the gain depends on the material, the type of cavities, as well as the wavelength λ and the direction Δ of the emitted or incident radiation. When grooves of dimensions larger than λ are fabricated in a sample, the models, taking into account the successive reflections on their inner sides, give a good agreement with experimental data. But a similar theory does not explain the substantial increase of the infrared emissivity of ballblasted samples.

KEY WORDS: directional spectral emissivity; macroroughness; microroughness; mechanical surface treatments; radiative properties.

1. INTRODUCTION

Radiative properties of an optically polished opaque material depend only on its temperature T, for an incident or emitted flux characterized by a wavelength λ and a direction Δ. The adjective "opaque" means that the material does not transmit any fraction of the incident monochromatic electromagnetic radiation; more restrictively, the penetration depth is supposed to be macroscopically small (less than a millimeter). The expression "optically polished" applies to a surface, the roughness of which is characterized by dimensions such as quadratic average heights σ, much smaller

[1]Groupe de Recherches Thermiques du C.N.R.S. associé à l'École Centrale des Arts et Manufactures, Grande Voie des Vignes, 92290 Châtenay-Malabry, France.

0195-928X/82/1200-0335$03.00/0

than the wavelength λ of the considered radiation ($\sigma \ll \lambda$), and by surface wavelengths long compared to λ. For these opaque and almost perfectly plane materials, the directional spectral factors may be deduced from the values of the indices of refraction and extinction; for given T, λ, and Δ, the emitted, reflected, or absorbed fluxes are readily determined.

In order to modify the radiative transfers, coatings may be applied that impose their own radiative characteristics. This happens spontaneously when oxide layers grow on the surface of heated metals. But the results are unforeseeable and not always in conformity with what was expected. Paints may be used to increase the emitted flux, for example; but ageing and adherence problems arise when the material is exposed to corrosive substances or subjected to temperature variations, etc.

Simple processes such as grooving (Section 3) or sandblasting (Section 4) produce cavities of diversified types. When their geometrical characteristics are larger than λ, the concept of "apparent" radiative properties can be introduced, which includes both emission and reflection on the inner sides of the cavities. In this paper, geometrical optics is used to compute these properties. The calculated values are compared with experimental results obtained with two experimental arrangements. Except for one case, the agreement is quite good. These processes may increase the hemispherical emissivities; they also allow the emission to be favored towards a given direction. Radiative transfers may be optimized, and no ageing problem occurs as the considered treatments are long-lasting, which is not the case for paints.

2. APPARENT RADIATIVE FACTORS OF A CAVITY

Let us recall that the radiative properties of an opaque material, the surface of which is optically smooth or slightly rough ($\sigma < \lambda$), are characterized by the following factors [1].

1. The directional spectral emissivity $\epsilon'_\lambda(\lambda, \Delta, T)$ is the ratio of the flux (Fig. 1) emitted by an elementary surface dS, in a solid angle $d\Omega$ around Δ and in the wavelength range $[\lambda, \lambda + d\lambda]$, to the one emitted by a blackbody under the same conditions. ϵ'_λ is a function of the wavelength λ, of the direction of emission $\Delta(\theta, \varphi)$ (symbolically noted by a prime $'$), and of the temperature T of dS.
2. If a flux is falling upon dS from the direction Δ in the range $d\lambda$, the directional spectral absorptivity $\alpha'_\lambda(\lambda, \Delta, T)$ represents the absorbed fraction and the directional-hemispherical spectral reflectivity $\rho'^{\frown}_\lambda(\lambda, \Delta, T)$ represents the fraction reflected towards all directions of a hemispherical envelope covering dS, (notation $\frown$).

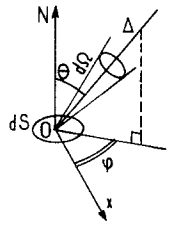

Fig. 1. Elementary surface dS emitting a flux towards the direction Δ or receiving a flux from the same direction. ON is the perpendicular to dS; Ox is the reference axis in the plane of dS; $d\Omega$ is the solid angle around Δ.

3. If the flux falling upon dS comes from all the directions within the half space surrounding dS, the fraction reflected in the direction Δ, within the solid angle $d\Omega$, is called the hemispherical-directional spectral reflectivity $\rho_\lambda^{\frown\prime}$. This factor is seldom employed as it depends on the spatial distribution of the incident flux [1]; it becomes of practical interest when this distribution is isotropic; the reflectivity is then noted $\rho_{\lambda\,\mathrm{iso.}}^{\frown\prime}(\lambda, \Delta, T)$.

The conservation of energy between the flux incident from the direction Δ on one hand and the fluxes reflected and absorbed on the other hand, as well as the conservation of the "black" radiation corresponding to the perfect thermodynamic equilibrium, lead, respectively, to the relations [2]

$$\alpha'_\lambda + \rho_\lambda^{\prime\frown} = 1 \tag{1a}$$

$$\epsilon'_\lambda + \rho_{\lambda\,\mathrm{iso.}}^{\frown\prime} = 1 \tag{1b}$$

In these conditions, Kirchhoff's law [1, 2] is represented by any of the relations

$$\epsilon'_\lambda(\lambda, \Delta, T) = \alpha'_\lambda(\lambda, \Delta, T) \tag{2a}$$

$$\rho_\lambda^{\prime\frown}(\lambda, \Delta, T) = \rho_{\lambda\,\mathrm{iso.}}^{\frown\prime}(\lambda, \Delta, T) \tag{2b}$$

Because of these relations, the determination of only one factor is sufficient to compute all the fluxes whether emitted, absorbed or reflected. Later on, we shall assume that the directional spectral emissivity $\epsilon'_\lambda(\lambda, \Delta, T)$ of the material of the inner side of the cavity is known and independent of the angle φ (Fig. 1). We note $\epsilon'_\lambda(\theta)$ with $\theta = (\Delta, 0N)$.

2.1. Conventions and Assumptions. Apparent Directional Spectral Emissivity

The cavities usually studied have a plane aperture, the surface of which is called "apparent surface" S_a (Fig. 2). The apparent directional spectral emissivity $\epsilon'_{\lambda a}(\Delta)$ of the cavity in the direction Δ is equal to the one that the plane surface S_a should have if it were materialized, to produce the same flux in the direction Δ; $\epsilon'_{\lambda a}(\Delta)$ is an average over the surface S_a as the flux, coming from the cavity and crossing S_a at M, is not uniform. This definition of $\epsilon'_{\lambda a}(\Delta)$ implies that the dimensions of the cavity are small compared to the distance it is observed from. Otherwise, the flux apparently "emitted" in the direction Δ, proportional to $\epsilon'_{\lambda a}(\Delta)$, is in fact an average, upon the surface S_p of the inner side, of the fluxes leaving each point Q. We call "leaving flux" the sum of the fluxes emitted and reflected at Q. If we note $L_\lambda(\Delta, Q) = L_\lambda(\Delta, M)$, the intensity of the leaving flux, $\epsilon'_{\lambda a}(\Delta)$ is equal to

$$\epsilon'_{\lambda a}(\Delta) = \frac{\int_{S_p} L_\lambda(\Delta, Q)\, dS_p}{L^0_\lambda(T) S_p} = \frac{\int_{S_a} L_\lambda(\Delta, M)\, dS_a}{L^0_\lambda(T) S_a} \tag{3}$$

For a blackbody, the intensity is independent of direction and is designated by $L^0_\lambda(T)$. The direction Δ is defined by two angles, noted γ and ψ, whatever cavities may be considered. For infinite length grooves (Sections 2 and 3) and for spherical caps (Section 4), γ and ψ do not have the same definition.

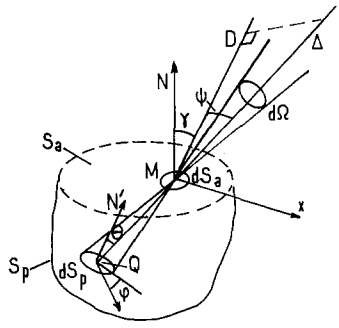

Fig. 2. The apparent surface, a nonmaterial plane of area S_a, limits the aperture of a cavity, the inner sides area of which is S_p. A flux leaves the point M towards the direction Δ. D is the perpendicular projection of Δ upon the plane (MN, Mx) with MN normal to S_a and the Mx reference axis of the S_a plane. Δ is defined by the angles (γ, ψ) with $\gamma = (D, MN)$ and $\psi = (\Delta, D)$.

The increase of the apparent emission of the cavity, compared to the one of the plane material of the inner side, is due to the successive reflections of the radiation inside the cavity. The use of the laws of geometrical optics to take into account the reflections implies that the wavelength λ is smaller than the dimensions of the cavity ($\lambda < \sigma$). This hypothesis is appropriate for most surfaces, except for infrared radiation and surface where $\sigma \simeq \lambda$ (Section 4). In other respects, instead of calculating $\epsilon'_{\lambda a}(\Delta)$, it is often easier to compute the absorbed fraction of directional flux incident upon the cavity; so $\alpha'_{\lambda a}(\Delta)$ is determined and, according to Kirchhoff's law [Eq. (2)],

$$\epsilon'_{\lambda a}(\Delta) = \alpha'_{\lambda a}(\Delta) \tag{4}$$

In Eq. (3) for $\epsilon'_{\lambda a}(\Delta)$, the intensity $L_\lambda(\Delta, Q) = L_\lambda(\theta, \varphi, Q)$ is the sum of the intensities of the fluxes emitted and reflected in Q; it is a function of the factors $\epsilon'_\lambda(\theta)$ and $\rho'^{\frown}_\lambda(\theta) = 1 - \epsilon'_\lambda(\theta)$. Calculation of $\epsilon'_{\lambda a}(\Delta)$ requires knowledge of the real value of the emissivity $\epsilon'_\lambda(\theta)$ and the law of reflection. Unfortunately, this law is usually rather complex and not well known. Only a few determinations of the bidirectional spectral reflectivity $\rho''_\lambda(\Delta, \Delta_r)$ exist, a quantity representing the fraction of a flux coming from a direction Δ and reflected towards Δ_r [1], [3]. Therefore, in order to compute $\epsilon'_{\lambda a}(\Delta)$, simplified radiative properties are used. We shall choose successively one of the three following hypotheses.

Hypothesis (*a*): *isotropic emission and diffuse isotropic reflection.* The emissivity $\epsilon'_\lambda(\theta)$ is independent of θ, and we write it ϵ_λ. Whatever the direction Δ of the incident flux may be, the reflected flux is distributed with the same intensity towards all the directions Δ_r of the space. In other words, ρ''_λ does not depend on Δ nor on Δ_r.

Hypothesis (*b*): *isotropic emission* (*emissivity* ϵ_λ) *and specular reflection.* The direction Δ_r of the reflected flux is determined by the direction Δ of the incident flux following Descartes' laws.

Hypothesis (*c*): *anisotropic emission and specular reflection.* The material emissivity $\epsilon'_\lambda(\theta)$ varies with θ. The law of variation may be reached through a direct measurement from a plane surface finished in the same way as the inner sides of the cavity. If this surface is optically polished, $\epsilon'_\lambda(\theta)$ may be computed from Fresnel's formulae [1]. We preferred the first method as the finish of the inner sides creates small roughnesses. However, for grazing incidence ($\theta > 80°$), measurements turn out to be difficult; thus, $\epsilon'_\lambda(\theta)$ is determined by making use of Fresnel's formulae, and this introduces no appreciable error.

For hypotheses (a) and (b), ϵ_λ, the hemispherical spectral emissivity, is

computed from the measured $\epsilon'_\lambda(\theta)$ through

$$\epsilon_\lambda = 2\int_0^{\pi/2} \epsilon'_\lambda \cos\theta \sin\theta \, d\theta \tag{5}$$

2.2. Infinite Length Groove: Apparent Pseudodirectional Spectral Emissivity

Some cavities (Fig. 3) such as the ∨-groove [4, 5, 6], ⊔-groove [7], ∪-groove [8], and ∩-groove [9], have already been studied. We also examined the combination of ∨ and ⊔ [10], that is, the ⋃-groove. For these grooves with infinite length, the direction Δ is defined (Fig. 4) by the two angles, $\gamma = (D, MN)$ and $\psi = (\Delta, D)$; NMx is a cross-section plane with MN perpendicular to S_a and Mx belonging to S_a. D is the projection of Δ upon the plane NMx. The apparent emissivity $\epsilon'_{\lambda a}(\Delta) = \epsilon'_{\lambda a}(\gamma, \psi)$, defined by Eq. (3), is a function of γ and ψ. Because of the particular geometrical properties of a groove, it is interesting to consider the elementary solid angle limited by the two half-planes $P(\gamma)$ and $P(\gamma + d\gamma)$; these planes form a dihedron, the ridge of which is located on an elementary strip of infinite length and of area dS_a per unit length. Instead of examining each direction Δ contained in the plane $P(\gamma)$, we may average the values of the emissivities $\epsilon'_{\lambda a}(\gamma, \psi)$ over all the directions of the plane $P(\gamma)$ and define an apparent pseudodirectional spectral emissivity $\epsilon^{\times}_{\lambda a}(\gamma)$. Let $L_\lambda(\gamma, \psi, M)$ be the intensity of the flux leaving M in each direction Δ; one can easily show [10] that

$$\epsilon^{x}_{\lambda a}(\gamma) = \int_{S_a} dS_a \int_{\psi=-\pi/2}^{\psi=+\pi/2} L_\lambda(\gamma, \psi, M) \cos^2\psi \, d\psi \Big/ \left(\frac{\pi}{2} L^0_\lambda S_a\right) \tag{6}$$

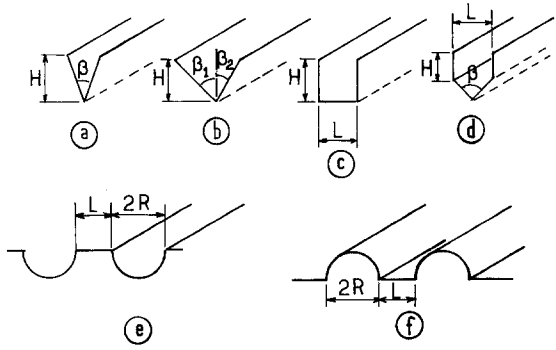

Fig. 3. Diagrams for some infinite length grooves: (a) symmetrical ∨-groove; (b) unsymmetrical ∨-groove; (c) ⊔-groove; (d) ⋃-groove; (e) concave circular groove; (f) convex circular groove.

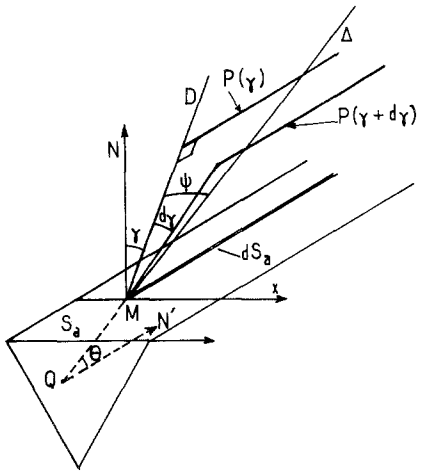

Fig. 4. Infinite length groove. The elementary apparent area per unit length is dS_a. Δ is a direction in the plane $P(\gamma)$. D is the perpendicular projection of Δ upon the cross-section plane (Mx, MN). For the computation of the apparent hemispherical emissivity $\epsilon_{\lambda a}$, we consider the solid angle limited by the two half planes $P(\gamma)$ and $P(\gamma + d\gamma)$.

Then the apparent hemispherical spectral emissivity, equal to that which would characterize the plane surface S_a, emitting a flux identical to the one produced by the groove towards all the directions Δ, is computed by the following equation:

$$\epsilon_{\lambda a} = \tfrac{1}{2}\int_{-\pi/2}^{+\pi/2} \epsilon_{\lambda a}^{\times}(\gamma)\cos\gamma\, d\gamma \tag{7}$$

In the cross-section of the groove, the apparent directional spectral emissivity is given by Eq. (3), that is,

$$\epsilon'_{\lambda a}(\gamma, \psi = 0) = \int_{S_a} L_\lambda(\gamma, \psi = 0, M)\, dS_a \Big/ \left(L_\lambda^0(T) S_a\right) \tag{8}$$

When the emission of the material is supposed to be isotropic [hypotheses (a) and (b)], the factors $\epsilon'_\lambda(\theta)$ or $\rho'^{\frown}_\lambda(\theta)$ are independent of the direction Δ considered. So, in order to compute $\epsilon'_{\lambda a}(\gamma, \psi)$, one has only to take into account the number of reflections undergone by a ray, irrespective of its direction. Therefore the path of a ray may be projected upon a cross-sectional plane [10]; in consequence, the angle ψ has no influence and

$$\epsilon'_{\lambda a}(\gamma, \psi) = \epsilon'_{\lambda a}(\gamma, \psi = 0) = \epsilon_{\lambda a}^{\times}(\gamma) \tag{9}$$

But, if the emission is anisotropic, even if the reflection is specular [hypothesis (c)], the emissivity $\epsilon'_\lambda(\theta)$ depends on the angle θ between Δ and the normal QN' to the inner side. θ is different from the angle between D and QN' (Fig. 4), so

$$\epsilon'_{\lambda a}(\gamma,\psi) \neq \epsilon'_{\lambda a}(\gamma,\psi=0), \qquad \epsilon'_{\lambda a}(\gamma,\psi) \neq \epsilon^{\times}_{\lambda a}(\gamma) \tag{10}$$

In the literature (for example, [4–9]), the computation is limited to the determination of $\epsilon'_{\lambda a}(\gamma,\psi=0)$. In the present study, we also calculated $\epsilon^{\times}_{\lambda a}(\gamma)$ in the case of hypothesis (c), in order to compare these two apparent emissivities; the results will be described below.

3. INFINITE LENGTH GROOVES: THEORETICAL AND EXPERIMENTAL RESULTS

3.1. Methods of Computation

First let us review briefly the main methods used and their assumptions.

The *iterative method* is based upon the solution of a linear integral equation [4, 7]. *The variational (or Rayleigh–Ritz) method* is based upon the solution of a system of coupled integral equations [11]. Both of these methods involve the notion of spectral radiosity [1]; consequently, the emission and the reflection of the inner side of the cavity have to be assumed isotropic [hypothesis (a)]. The *image method* implies a specular law of reflection. The emission is usually assumed to be isotropic [4, 7] [hypothesis (b)]; but it is possible to take into account an anisotropic emission [hypothesis (c)] [12], especially if the computation is limited to the determination of $\epsilon'_{\lambda a}(\gamma,\psi=0)$.

The use of any of these methods leads to the radiative properties of a cavity. Figure 5 shows that a $\vee$-groove substantially increases the emissivity in the direction perpendicular to the apparent surface; otherwise, the aspect of the curves $\epsilon'_{\lambda a}(\gamma,\psi=0)$ depends on the hypothesis made upon the laws of reflection.

The application of the Monte Carlo method to the determination of apparent factors is given in ref. [10]. The radiative energy leaving each component of the system is quantified in the "photon pack," or in shorter form, "photon." Each photon transports the same quantity of energy; it is followed during all its "lifetime" from its emission until its absorption or its exit out of the cavity. As the method lies upon the direct simulation of the phenomenon by statistical sampling, its results depend on the number of photons used, called the "size" of the sampling. The size has to be large enough so that the uncertainty of the results could be considered as

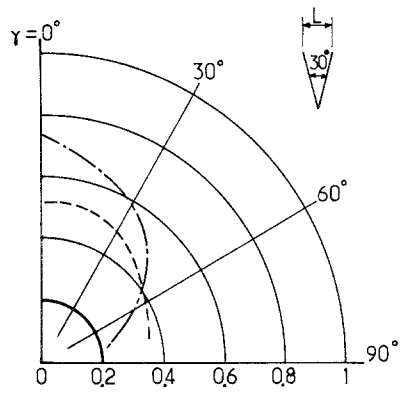

Fig. 5. Apparent directional spectral emissivity $\epsilon'_{\lambda a}(\gamma, \psi = 0)$ for a $\vee$-groove with vertex angle $\beta = 30°$. The width L has no influence upon the results. The hemispherical spectral emissivity of the inner sides is $\epsilon_\lambda = 0.20$. Dashed curve, iterative method [hypothesis (a)]; dot-dashed curve, image method [hypothesis (b)].

acceptable. However, up to now, no mathematical criterion has been set to determine *a priori* the right size. In any event, computation time is larger for this method than for the others, but it may be reduced by using special methods [10] such as approximation of implicit expressions by functions, choice of the factor to be calculated ($\alpha^{\times}_{\lambda a}$ instead $\epsilon^{\times}_{\lambda a}$), use of subroutines to generate random numbers, etc.

On the other hand, the Monte Carlo method presents some advantages; in particular, it is well suited to problems of radiative exchange when the effective behavior of the materials for both reflection and emission has to be taken into account. As it is not submitted to any restrictive hypothesis, it may always be compared to other methods; the examples, presented in ref. [10], show a good agreement. Moreover, the same computational structure may be conserved whatever the hypothesis [(a), (b), or (c) above, for example].

Studies on $\vee$-grooves [4, 5] or $\sqcup$-grooves [7, 12] show that these cavities have complementary actions. The first type increases emission in the direction normal ($\gamma = 0°$) to the apparent surface (Fig. 5), while the second type increases the emission towards the tangential direction ($\gamma = 90°$) when the reflection is specular (see Fig. 10 below). So a $\cup$-groove, which associates both of these grooves, should have an important apparent emissivity $\epsilon'_{\lambda a}(\gamma)$ whatever angle γ is considered. The curves of Fig. 6, computed by the Monte Carlo method with hypotheses (a), (b), and (c), show that the ratio $\epsilon^{\times}_{\lambda a}(\gamma)/\epsilon'_\lambda$ is generally larger than 2. The directional spectral emissivity ϵ'_λ, measured for the material of the inner side of the cavity (Fig. 6), is used for the computation of $\epsilon^{\times}_{\lambda a}(\gamma)$ in the case of

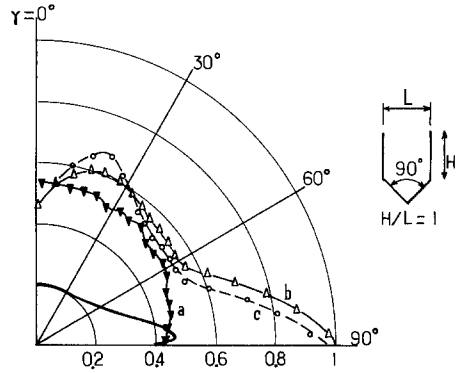

Fig. 6. Apparent pseudodirectional emissivity $\epsilon_{\lambda a}^{\times}(\gamma)$ vs. γ for a $\cup$-groove. The computation is based on the Monte Carlo method. Curve ▼ is hypothesis (a) with $\epsilon_\lambda = 0.22$. Curve △ is hypothesis (b) with $\epsilon_\lambda = 0.22$. Curve ○ is hypothesis (c); the directional spectral emissivity $\epsilon'_\lambda(\theta = \gamma)$ of the material (304 L stainless steel), measured at $T = 773$ K, $\lambda = 5$ μm, is given by the continuous line curve without points.

hypothesis (c). The value of the hemispherical spectral emissivity of the material, Eq. (5), is $\epsilon_\lambda = 0.22$. The importance of the reflection law is emphasized once again. On the other hand, the curves corresponding to hypotheses (b) and (c) are quite similar. This was to be expected since the anisotropy of emission is only noticeable for angles θ larger than 60°; for these angles, the fluxes emitted are low as they are proportional to $\cos\theta$.

The Monte Carlo method allows the comparison between the pseudo-directional spectral emissivity $\epsilon_{\lambda a}^{\times}(\gamma)$ and $\epsilon'_{\lambda a}(\gamma, \psi = 0)$, computed for the

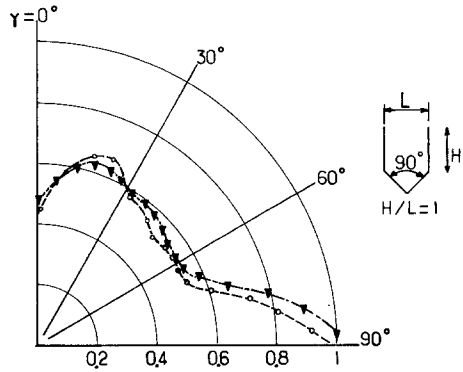

Fig. 7. Comparison of two Monte Carlo method results in the case of hypothesis (c). $\epsilon'_\lambda(\theta = \gamma)$ is the same as in Fig. 6. Curve ○, apparent pseudodirectional emissivity $\epsilon_{\lambda a}^{\times}(\gamma)$; Curve ▼, apparent directional emissivity in the cross-section plane $\epsilon'_{\lambda a}(\gamma, \psi = 0)$.

cross-sectional plane. Following formula (9), these two emissivities have the same value if the material emission is isotropic, and this is true for isotropic or specular reflection. We note in Fig. 7 that these emissivities remain almost equal in the case of anisotropic emission [hypothesis (c)] for the reason quoted above. So a close estimate of the results can be found by assuming that the emission is isotropic; therefore the ray tracing can be done in the straight section plane.

The cavity effect is usually characterized by the ratio between the hemispherical spectral emissivities $\epsilon_{\lambda a}$, Eq. (7), and ϵ_λ, Eq. (5); we designate this ratio by

$$\eta = \frac{\epsilon_{\lambda a}}{\epsilon_\lambda} \tag{11}$$

Figure 8 gives, for a particular type of groove and various ratios L/H, the variation of η as a function of the hemispherical spectral emissivity ϵ_λ of the cavity material. We note that the efficiency of the cavity is quite important for low ϵ_λ. When ϵ_λ tends to zero, η tends to S_p/S_a (S_p is the inner side area and S_a the apparent area). Besides, the lower the L/H ratio, the stronger the cavity effect. Emissivity or absorptivity of a material may be tripled or quadrupled by a $\cup$-grooving.

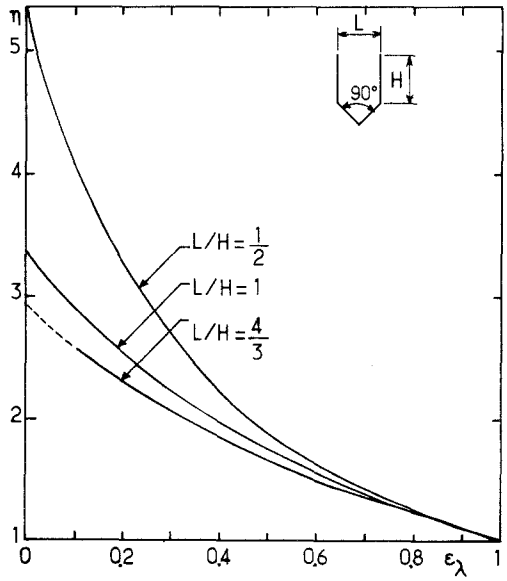

Fig. 8. Cavity effect. $\eta = \epsilon_{\lambda a}/\epsilon_\lambda$ is given as a function of the hemispherical emissivity of the material. The calculation is done using the Monte Carlo method with hypothesis (b).

3.2. Comparison of Theoretical and Experimental Results

3.2.1. Experimental Technique

In order to measure the "apparent" characteristics, $\epsilon'_{\lambda a}(\gamma, \psi)$ or $\epsilon_{\lambda a}(\gamma, \psi = 0)$, the flux in the direction Δ may be observed using a single large cavity or a grooved sample. The first technique has to be chosen if the apparent emissivity at each point M of S_a (Fig. 1) has to be measured. However, the emissivity $\epsilon'_{\lambda a}(\Delta) = \epsilon'_{\lambda a}(\gamma, \psi)$, defined in Eq. (3), is an average over S_a, and the second technique we adopted leads to a better determination of this factor. The width and the depth of each groove are small compared to the length so that it may be considered as isothermal; the standard dimensions of samples are $200 \times 100 \times 12$ mm. The experiments are conducted at $T \simeq 700$ K, at a wavelength λ close to $\lambda_m(T)$; $\lambda_m(T)$ corresponds to the maximum of the emission of the blackbody at this temperature, that is, between 4 and 5 μm. The measured fluxes are large enough so that the relative error in the results is lower than 3%.

The experimental arrangement allows us to aim at an area of the sample large enough to include a great number of grooves. The ratio between the flux leaving the sample in the direction $\Delta(\gamma, \psi)$ and the flux emitted by a blackbody is equal to the measured emissivity $\epsilon'_{\lambda\ \text{meas.}}(\gamma, \psi)$. When the grooves of width L are separated by plane zones of width L' and of emissivity $\epsilon'_\lambda(\gamma)$, $\epsilon'_{\lambda\ \text{meas.}}(\gamma, \psi)$ depends on the ratio L'/L since

$$\epsilon'_{\lambda\ \text{meas.}}(\gamma, \psi) = \frac{\epsilon'_{\lambda a}(\gamma, \psi) + (L'/L)\epsilon'_\lambda(\gamma)}{1 + (L'/L)} \tag{12}$$

The experimental arrangement has been described in previous publications [3, 9, 12]. The target area, defined by the optical setup, is included in the aperture of the blackbody of diameter 22 mm. The monochromator is a Perkin-Elmer spectrometer. The optical bench includes a spherical mirror which focuses the flux leaving the sample or the blackbody into the entrance slit of the spectrometer. A second spherical mirror creates an image of the exit slit on a Ge-Au detector. A polarizer is introduced in the optical path so that the emissivities $\epsilon'_{\lambda //}$ and $\epsilon'_{\lambda \perp}$, corresponding to the two classical planes of polarization, are measured; the average $\epsilon'_\lambda = (\epsilon'_{\lambda //} + \epsilon'_{\lambda \perp})/2$ is then computed [13]. The use of a chopper and a lock-in amplifier eliminates most of parasitic radiations, except for the fluxes reflected by the sample, which are the main causes of error [13, 14]. The use of two regulators reduces to 2 K the residual gap between the temperatures of the sample and of the blackbody.

3.2.2. *Advantages of Some Grooves*

Figure 9 represents the emissivities of a plane material sample and of a $\cup$-grooved sample of 304 L stainless steel at 773 K. The Monte Carlo computed results [hypothesis (c)] agree with experimental data, obtained with the first experimental arrangement made in our Laboratory [9, 12]; its precision, about 10%, was not as good as the present one, which is 3% as stated above. Moreover, the reflection of the inner sides may not have been perfectly specular. Fig. 9 shows that grooving substantially increases emissivity, which is almost doubled in all directions in spite of plane zones.

Emission towards a given direction may be increased by grooving; for example, for a specular reflection of the material:

1. A $\sqcup$-groove (Fig. 10) gives an apparent emissivity $\epsilon'_{\lambda a}(\gamma, \psi = 0)$ which increases with γ and tends to 1 for $\gamma = 90°$. The correspondence between the experimental and image theory computed [hypothesis (c)] values is still reasonable; the differences are probably due to the reasons mentioned above.
2. An unsymmetrical $\vee$-groove (Fig. 11) modifies the direction of the maximum of the emissivity. Although emission is assumed to be isotropic [hypothesis (b)], the image method computed values are in good agreement with the experimental values.

If the $\vee$-groove is broadly opened (Fig. 12), the emissivity becomes more isotropic than for the plane material; $\epsilon'_{\lambda a}(\gamma, \psi = 0)$ does not vary very much

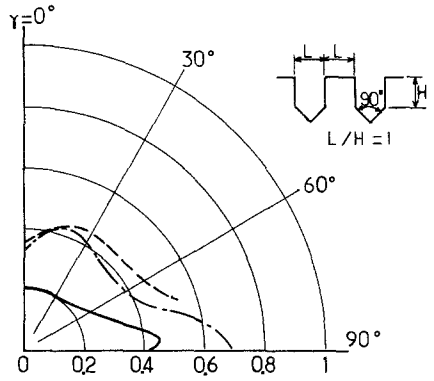

Fig. 9. Comparison between the measured emissivities $\epsilon'_{\lambda\ \text{meas.}}(\gamma, \psi = 0)$ at $T = 773$ K, $\lambda = 5$ μm and the calculated emissivities $\epsilon'_{\lambda\ \text{calc.}}(\gamma, \psi = 0) = [\epsilon'_{\lambda a}(\gamma, \psi = 0) + \epsilon'_{\lambda}(\gamma)]/2$ for a 304 L stainless steel sample with $\cup$-grooves and plane regions. The value of L and H (2 mm) has no influence upon the results. Solid curve, directional spectral emissivity $\epsilon'_{\lambda}(\gamma)$ of a plane sample. Dot-dashed curve, apparent directional emissivity $\epsilon'_{\lambda\ \text{calc.}}(\gamma, \psi = 0)$ computed by the Monte Carlo method with hypothesis (c). Dashed curve, measurements of $\epsilon'_{\lambda\ \text{meas.}}(\gamma, \psi = 0)$.

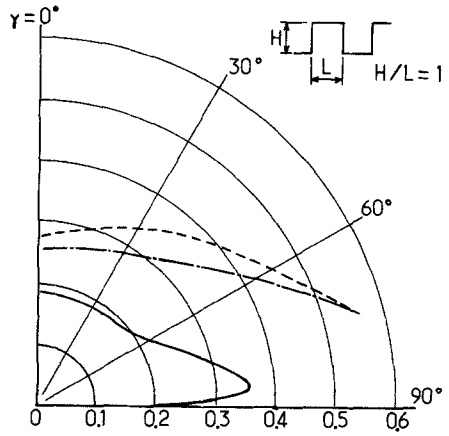

Fig. 10. Comparison between the measured emissivities $\epsilon'_{\lambda\,\text{meas.}}(\gamma, \psi = 0)$ at $T = 573$ K, $\lambda = 4.5$ μm, and the calculated emissivities $\epsilon'_{\lambda\,\text{calc.}}(\gamma, \psi = 0) = [\epsilon'_{\lambda a}(\gamma, \psi = 0) + \epsilon'_{\lambda}(\gamma)]/2$ for a 304 L stainless steel sample with ⊔-grooves and plane regions. Solid curve, directional spectral emissivity $\epsilon'_{\lambda}(\gamma)$ of a plane sample. Dot-dashed curve, apparent directional emissivity $\epsilon'_{\lambda\,\text{calc.}}(\gamma, \psi = 0)$ computed by the image method with hypothesis (c). Dashed curve, measurements of $\epsilon'_{\lambda\,\text{meas.}}(\gamma, \psi = 0)$.

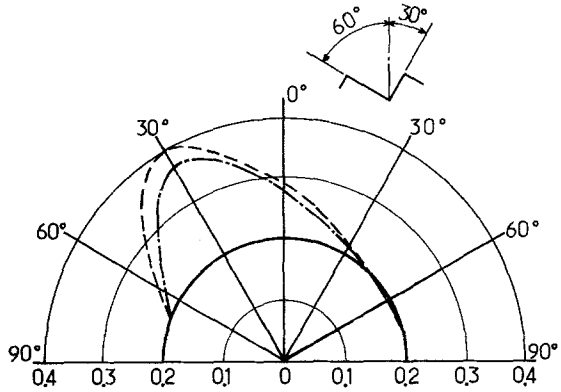

Fig. 11. Comparison between the apparent directional emissivities, measured, $\epsilon'_{\lambda\,\text{meas.}}(\gamma, \psi = 0)$, at $T = 573$ K, $\lambda = 4.5$ μm, and calculated $\epsilon'_{\lambda a}(\gamma, \psi = 0)$, for a 304 L stainless steel sample with unsymmetrical ∨-grooves. Dot-dashed curve, $\epsilon'_{\lambda a}(\gamma, \psi = 0)$, computed by the image method with hypothesis (b) and a hemispherical emissivity of the material: $\epsilon_{\lambda} = 0.21$. Dashed curve, measurements of $\epsilon'_{\lambda\,\text{meas.}}(\gamma, \psi = 0)$.

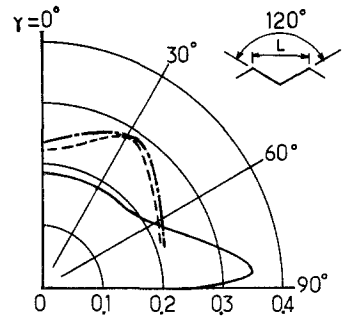

Fig. 12. Comparison between the apparent directional emissivities, measured, $\epsilon'_{\lambda\ \mathrm{meas.}}(\gamma, \psi = 0)$, at $T = 573$ K, $\lambda = 4.5$ μm, and calculated, $\epsilon'_{\lambda a}(\gamma, \psi = 0)$, for a 304 L stainless steel sample with symmetric $\vee$-grooves. Solid curve, directional spectral emissivity $\epsilon'_{\lambda}(\gamma)$ of a plane sample. Dot-dashed curve, $\epsilon'_{\lambda a}(\gamma, \psi = 0)$, computed by the image method with hypothesis (c). Dashed curve, measurements of $\epsilon'_{\lambda\ \mathrm{meas.}}(\gamma, \psi = 0)$.

with γ as is demonstrated by experimental as well as theoretical results [hypothesis (c)].

As shown by the examples presented, an adequate grooving of surfaces may be of practical interest when emission has to be increased or a particular direction has to be favored. Furthermore, they illustrate the good agreement between experiments and theories, the Monte Carlo method in particular; however, the exact radiative characteristics have to be used to compute an accurate evaluation of $\epsilon'_{\lambda a}(\gamma, \psi)$ and $\epsilon^{\times}_{\lambda a}(\gamma)$. Such a good agreement has been observed because the same machine finishing was applied to the inner sides of the grooves and to the plane surface. For small roughnesses it is impossible to obtain the same surface state for the inner sides of cavities and for the plane sample; therefore the agreement between experiments and theories is not as good.

4. STUDY OF SPHERICAL-CAP CAVITIES: APPLICATION TO SANDBLASTED, SHOTBLASTED, AND BALLBLASTED SURFACES

Superficial treatments such as milling or sandblasting produce small roughnesses and substantially modify radiative properties of materials. Many theories [13] have been proposed to explain their influence; two main approaches are used. The first, based on diffraction theory, presents a gap: it doesn't take into account multiple reflections or mask effects [13, 15], though they have a great influence for very rough samples. The second,

based on the laws of geometrical optics, is applicable when the dimensions characterizing the roughness (σ) are larger than the wavelength λ of the radiation ($\sigma > \lambda$) or are of the same order ($\sigma \simeq \lambda$). We shall limit ourselves to the second approach. For our experimental conditions, in the visible range, σ will be larger than λ, whilst in the infrared range, σ and λ will be of the same order.

A rough surface has to be represented by a distribution of variously dimensioned cavities, the geometry of which has to be properly chosen. For machined surfaces where a direction is favored, $\vee$-grooves or semicircular grooves are well adapted, but they can't account for sandblasted surfaces. Three-dimensional models with pyramidal [16] or spherical [17] asperities are also unsatisfactory. Scanning electronic microscope pictures show that these treatments, especially ballblasting, produce concave spherical cap cavities on the surface of the sample (Fig. 13). In order to study the influence of this type of roughness, the apparent directional spectral emissivity of a spherical cap cavity has to be computed, and a statistical distribution of the cavities has to be adopted.

The cavities are created by the projection of various particles: small grains of white corundum (sandblasting), regular spherical balls of glass (ballblasting), or small irregular particles of steel (shotblasting). The inner sides of cavities are not as well finished as the grooves discussed above (Section 3). As it is impossible to measure their exact radiative characteristics, we shall adopt those characterizing the optically smooth material, that is, anisotropic emission and specular reflection [hypothesis (c)]. However, as the inner sides are probably not smooth, the agreement between theory and experiment should not be expected to be as good as in Section 3.

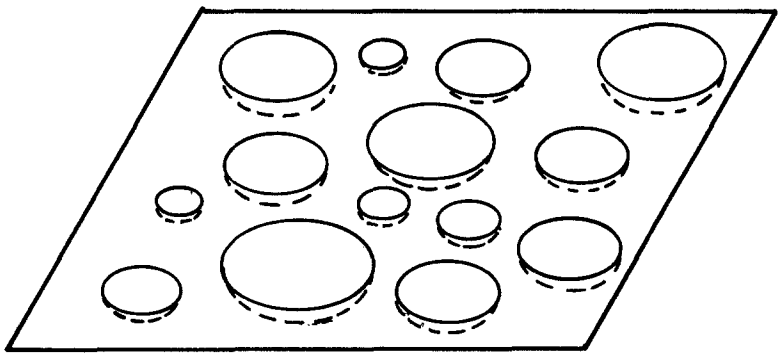

Fig. 13. Representation of ballblasted surfaces by spherical caps of varied characteristics.

4.1. Apparent Directional Spectral Emissivity of a Concave Spherical Cap

Let us take a spherical cap inscribed in a sphere of center O and radius R (Fig. 14a). It is characterized by δ, the complementary of its vertex half-angle, which we shall call the aperture. A direction Δ (Figs. 14b and c) is defined by the angles $\gamma = (\Delta, MN)$ and $\psi = (OP, PX)$. P is the intersection of Δ with the circle of center O, traced in the plane parallel to S_a. PX is the projection of Δ upon this circle. In the plane xOy, P is located by its polar coordinates $OP = r$ and ψ.

Let us consider an incident ray in the direction Δ. After a specular reflection from the inner side of the cap at a point Q, the reflected ray remains in the plane π defined by PQ and the normal in Q, that is, OQ. So π is determined by the three points O, P, Q, or by O and the line Δ. A second reflection may occur at a point Q'; QQ' is still in the plane π as well as the normal OQ'. So any reflected ray belongs to the diametral plane π (Fig. 14d). The intersection of π with the cap is an arc of circle II' characterized by the aperture δ'. The angle between Δ and the axis of symmetry of this arc is γ'. One can easily find [18]

$$\delta' = \arcsin\left(\sin\delta \frac{\cos\gamma'}{\cos\gamma}\right) \tag{13}$$

$$\gamma' = \arcsin(\sin\gamma\cos\psi) \tag{14}$$

The angles of incidence and reflection are constants and equal to

$$\theta = \arcsin\left(\frac{r}{R}\cos\gamma'\right) \tag{15}$$

For a given point P and a direction Δ, the apparent directional emissivity or absorptivity is

$$\begin{aligned}\epsilon'_{\lambda a}(P,\Delta) &= \alpha'_{\lambda a}(P,\Delta) \\ &= \alpha'_\lambda(\theta) + \alpha'_\lambda(\theta)\left[1 - \alpha'_\lambda(\theta)\right] + \cdots + \alpha'_\lambda(\theta)\left[1 - \alpha'_\lambda(\theta)\right]^{n-1}\end{aligned} \tag{16}$$

or

$$\epsilon'_{\lambda a}(P,\Delta) = \epsilon'_{\lambda a}(r,\gamma,\psi) = 1 - \left[1 - \alpha'_\lambda(\theta)\right]^n \tag{17}$$

where n is the number of reflections in the cap, and $\alpha'_\lambda(\theta) = \epsilon'_\lambda(\theta)$ is the

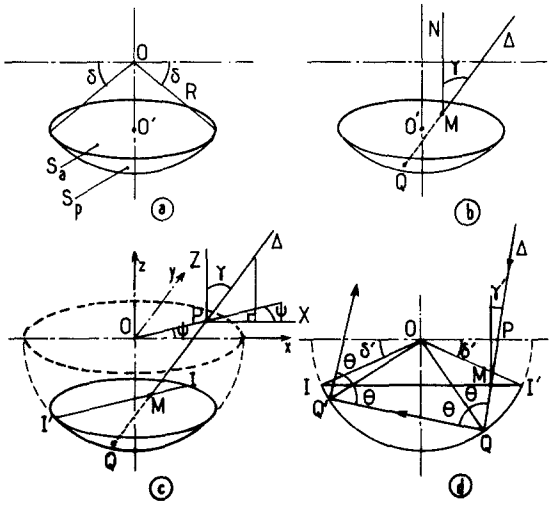

Fig. 14. (a) Definition of the parameters δ, R. (b) and (c) Definition of the angles γ and ψ that characterize the direction Δ; the diametral plane π, defined by O and Δ, cuts the spherical cap following a circular sector IQI'. (d) Diagram of the successive reflections at Q, Q', . . . , in the plane $\pi(O, \Delta)$.

directional spectral absorptivity (or emissivity) of the optically smooth material. The averaging of $\epsilon'_{\lambda a}(r, \gamma, \psi)$ over S_a, Eq. (3), leads to an apparent directional emissivity given by

$$\epsilon'^{\delta}_{\lambda a}(\gamma) = \frac{1}{\pi R^2 \cos^2\delta} \int_{\psi}\int_{r} \epsilon'_{\lambda a}(r, \gamma, \psi) r \, d\psi \, dr \tag{18}$$

After integration, it appears that $\epsilon'^{\delta}_{\lambda a}(\gamma)$ is independent of R and ψ; this last result could have been expected as the cap is symmetric. $\epsilon'^{\delta}_{\lambda a}(\gamma)$ depends on the aperture δ, denoted by the superscript δ.

To finish the computation, the number n of reflections undergone by a ray incident at P in the direction Δ is calculated [18, 19], from

$$n = E\left[\frac{\pi - \gamma' - \delta'}{2 \arccos((r/R)\cos\gamma')} + \frac{1}{2} \right] \tag{19}$$

E means the integer part of the expression between brackets. In other words, the number of reflections undergone is increased from n to $n + 1$ when $r = r_n$ with

$$r_n = \frac{R}{\cos\gamma'} \cos\left(\frac{\pi - \gamma' - \delta'}{2n + 1} \right) \tag{20}$$

Because n changes by steps, the integral in r has to be decomposed as follows:

$$\epsilon'^{\delta}_{\lambda a}(\gamma) = \frac{2}{\pi R^2 \cos^2\delta} \int_{\psi=0}^{\psi=\psi_L} \sum_{n=1}^{n=n_l+1} \int_{r_{n-1}}^{r_n} \epsilon'_{\lambda a}(r, \gamma, \psi) r \, dr \, d\psi \tag{21}$$

Integration or summation boundaries ψ_L, $n_l + 1$, r_0, and r_{n_l+1} are given by the geometrical intersection conditions of Δ and S_a. We have

$$\psi_L = \pi \qquad \text{for} \quad \delta + \gamma < \frac{\pi}{2} \tag{22a}$$

$$\psi_L = \arcsin(\operatorname{cotg}\gamma \operatorname{cotg}\delta) \qquad \text{for} \quad \delta + \gamma \geqslant \frac{\pi}{2} \tag{22b}$$

$$n_l + 1 = E\left[\frac{\pi - \gamma' - \delta'}{2|\gamma' - \delta'|} + \frac{1}{2} \right] \tag{22c}$$

$$r_0 = 0 \qquad \text{for} \quad \delta + \gamma < \frac{\pi}{2} \tag{22d}$$

$$r_0 = \frac{R}{\cos\gamma'} \cos(\pi - \gamma' - \delta') \qquad \text{for} \quad (\delta + \gamma) \geqslant \frac{\pi}{2} \tag{22e}$$

$$r_{n_l+1} = \frac{R\cos(\gamma' - \delta')}{\cos\gamma'} \tag{22f}$$

Numerical computation of $\epsilon'^{\delta}_{\lambda a}(\gamma)$ has been performed for spherical caps of 304 L stainless steel for two sets of conditions: $\lambda = 0.6$ μm, $T = 300$ K, and $\lambda = 5$ μm, $T = 773$ K. The emissivity $\epsilon'_\lambda(\theta)$ of the optically smooth material, as well as the apparent emissivity $\epsilon'^{\delta}_{\lambda a}(\gamma)$, are represented in Fig. 15. For a hemispherical cap ($\delta = 0$), the ratio $\epsilon'^{\delta=0}_{\lambda a}/\epsilon'_\lambda$ is much larger than 1 for an almost normal incidence direction; but it decreases for larger angles of incidence so that, within the infrared range, the apparent emissivity of the cap is more isotropic than the emissivity of the smooth sample. When δ is less than 40°, $\epsilon'^{\delta}_{\lambda a}(\gamma)$ tends to be $\epsilon'_\lambda(\gamma)$.

The cavity effect η, equal to the ratio $\epsilon^{\delta}_{\lambda a}/\epsilon_\lambda$ of the hemispherical emissivities, Eq. (11), may be calculated from Eq. (21) after an integration as in formula (5). But it is easier to compute η within the frame of hypothesis (a) or (b), as has been done in the literature. Analytical expressions for η are then obtained and the influence of reflection laws is put

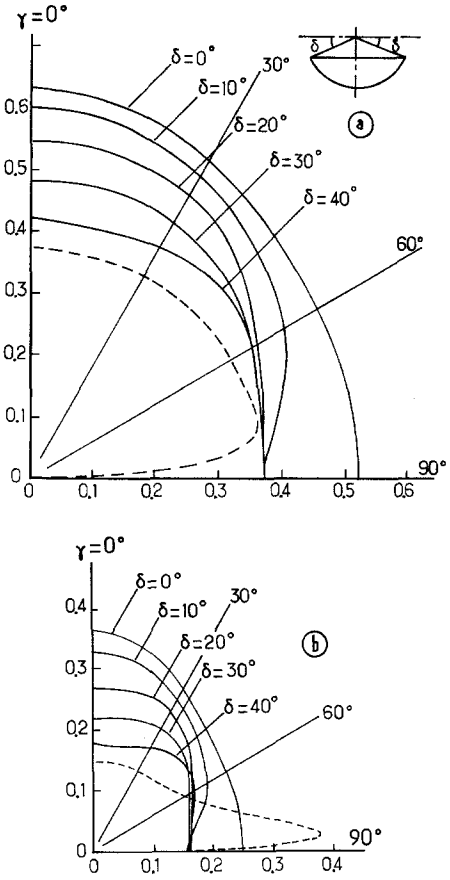

Fig. 15. Apparent directional spectral emissivity $\epsilon'^{\delta}_{\lambda a}(\gamma)$ of a spherical cap characterized by δ. The inner sides are made of 304 L stainless steel in the following cases: (a) $\lambda = 0.6$ μm, $T = 300$ K; (b) $\lambda = 5$ μm, $T = 773$ K. Dashed curves, directional spectral emissivity $\epsilon'_{\lambda}(\gamma)$ measured for a smooth sample. Solid curves, apparent directional spectral emissivity $\epsilon'^{\delta}_{\lambda a}(\gamma)$ calculated for various values of δ.

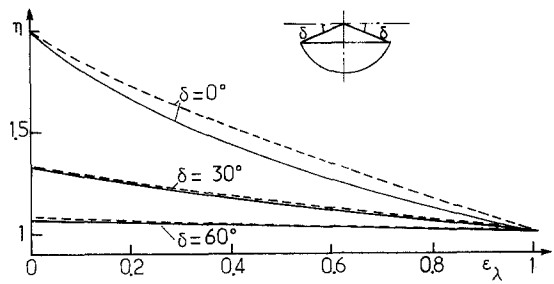

Fig. 16. Cavity effect $\eta = \epsilon^{\delta}_{\lambda a}/\epsilon_{\lambda}$ is given as a function of the hemispherical emissivity ϵ_{λ} of the material. The calculation was done in the case of hypothesis (a), solid curve; or (b), dashed curve.

forward. It is found:

For a diffuse isotropic reflection [*hypothesis* (*a*)] [8]:

$$\eta_d = \frac{1}{1 - (1 - \epsilon_\lambda)\left(\frac{1 - \sin\delta}{2}\right)} \tag{23}$$

For a specular reflection [*hypothesis* (*b*)] [5, 18]:

$$\eta_s = \frac{2}{1 + \sin\delta} - \epsilon_\lambda \frac{1 - \sin\delta}{1 + \sin\delta} \sum_{k=0}^{\infty} \frac{(1 - \epsilon_\lambda)^k}{(k+1)^2} \tag{24}$$

The curves, traced in Fig. 16 for various values of δ, show that η_d and η_s are not very different for $\delta = 0°$ and are almost equal for $\delta = 30°$ or $60°$. As for infinite length grooves, the cavity effect is all the more important as the cap is closed (small δ) and the emissivity ϵ_λ of the material is small. As is expected, η_d and η_s tend to approach S_p/S_a when ϵ_λ approaches zero.

4.2. Directional Spectral Emissivity of a Rough Surface Simulated by the Spherical-Cap Cavities Model

As stated above, some rough surfaces may be modelled by the juxtaposition of spherical caps (Fig. 13) of various sizes and depths, which we shall characterize by the parameters R and δ. The plane regions between the caps correspond to caps with δ tending to 90° and R to infinity. A direction Δ is defined by the angle γ with the normal to the apparent surface, which is common to all the cavities.

Let us call $\epsilon'_{\lambda r}(\gamma)$ the directional spectral emissivity of the rough surface and $p(R,\delta)\,dR\,d\delta$ the probability for a point M to belong to the apparent surface of a spherical cap, the radius of which is between R and $R + dR$, and the aperture of which is between δ and $\delta + d\delta$. $\epsilon'_{\lambda r}(\gamma)$ is inferred from $\epsilon'^{\delta}_{\lambda a}(\gamma)$ in Eq. (18) by

$$\epsilon'_{\lambda r}(\gamma) = \int_{\delta=0}^{\delta=\pi/2} \epsilon'^{\delta}_{\lambda a}(\gamma)\,d\delta \int_{R=0}^{\infty} p(R,\delta)\,dR \tag{25}$$

As $\epsilon'^{\delta}_{\lambda a}(\gamma)$ is independent of R, the integral over R represents the probability density $p(\delta)$ of the variable δ, that is, $p(\delta)\,d\delta$ is the probability for a point M to belong to the apparent surface of a spherical cap, the aperture of which is between δ and $\delta + d\delta$, whatever the radius R may be. Then

$$\epsilon'_{\lambda r}(\gamma) = \int_{\delta=0}^{\delta=\pi/2} \epsilon'^{\delta}_{\lambda a}(\gamma) p(\delta)\,d\delta \tag{26}$$

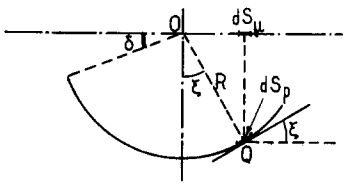

Fig. 17. Slope $\mu = tg\xi$ at each point Q of the inner side of the spherical cap.

Physical models as Beckmann's model [20] show that, for roughness dimensions larger than the wavelength ($\sigma > \lambda$), the important parameter is the quadratic average slope m of the surface. Here the slope at each point Q of the spherical cap is (Fig. 17): $\mu = tg\xi$; so we put

$$m = \bar{\mu} = tg\bar{\xi} \tag{27}$$

For a given cap of aperture δ, the slope distribution, that is, the probability $p_\delta(\mu)\,d\mu$ for the slope at Q to be between μ and $\mu + d\mu$, is equal to the ratio of the apparent elementary area dS_μ at Q to the apparent total area of the cap: $\pi R^2 \cos^2\delta$; so

$$p_\delta(\mu) = \frac{\mu}{\cos^2\delta(1+\mu^2)^2} \qquad \text{for} \quad 0 \leqslant \mu < \operatorname{cotg}\delta \tag{28a}$$

$$p_\delta(\mu) = \frac{-\mu}{\cos^2\delta(1+\mu^2)^2} \qquad \text{for} \quad -\operatorname{cotg}\delta < \mu \leqslant 0 \tag{28b}$$

$$p_\delta(\mu) = 0 \qquad \text{for} \quad \mu > \operatorname{cotg}\delta \quad \text{or} \quad \mu < -\operatorname{cotg}\delta \tag{28c}$$

The probability density $p_\delta(\mu)$ is independent of R; for a given aperture δ, the slope distribution does not depend on the size of the cap. Now let us consider the probability

$$p_{\delta,R}(\mu)\,d\mu\,dR\,d\delta = p(R,\delta)\,dR\,d\delta\,p_\delta(\mu)\,d\mu \tag{29}$$

to find a point Q where the slope is between μ and $\mu + d\mu$, in a cap, the radius of which is between R and $R + dR$, and the aperture of which is between δ and $\delta + d\delta$. Let us integrate the formula (29) for all the values of R and δ; the slope distribution $p(\mu)$ of the rough surface is then obtained to be

$$p(\mu) = \int_{\delta=0}^{\operatorname{arccotg}\mu} p(\delta)p_\delta(\mu)\,d\delta \tag{30}$$

$p_\delta(\mu)$ is given by Eq. (28). Now if we choose a $p(\mu)$ distribution, $p(\delta)$ is calculated [18] from Eq. (30). We give two examples.

For a gaussian slope distribution,

$$p(\mu) = \frac{1}{m\sqrt{2}} \exp\left(- \frac{\mu^2}{2m^2} \right) \tag{31}$$

the aperture distribution is

$$p(\delta) = \frac{1}{m\sqrt{2\pi}} \left[4 - \frac{3}{\sin^2\delta} + \frac{\cos^2\delta}{m^2 \sin^2\delta} \right] \frac{1}{\sin^2\delta} \exp\left(- \frac{\operatorname{cotg}^2\delta}{2m^2} \right) \tag{32}$$

with the condition

$$m \leqslant 1 \quad \text{or} \quad \bar{\xi} \leqslant 45° \tag{33}$$

so that $p(\delta)$ is always positive. Even with small aperture caps, the proportion of weak slopes remains important and high values of average slopes are not found.

For an exponential slope distribution,

$$p(\mu) = \frac{1}{m\sqrt{2}} \exp\left(- \frac{\mu\sqrt{2}}{m} \right) \qquad \text{for} \quad \mu \geqslant 0 \tag{34}$$

the aperture distribution is

$$p(\delta) = \frac{1}{m\sqrt{2}} \left[4 - \frac{3}{\sin^2\delta} + \frac{\sqrt{2}\cos\delta}{m \sin^3\delta} \right] \frac{1}{\sin^2\delta} \exp\left(- \frac{\sqrt{2}\operatorname{cotg}\delta}{m} \right) \tag{35}$$

with the condition

$$m \leqslant \sqrt{\frac{2}{6\sqrt{3} - g}} \quad \text{or} \quad \bar{\xi} \leqslant 50.16° \tag{36}$$

The average, given by Eq. (26), of the apparent directional emissivities $\epsilon'^{\delta}_{\lambda a}(\gamma)$, computed through formula (21) and weighted by a probability $p(\delta)$ given by Eq. (32) or (35), is calculated by making use of the trapezoidal rule. In spite of the appreciable differences between the two distributions of the caps, $p(\delta)$ has little influence upon the curves representing $\epsilon'_{\lambda r}(\gamma)$ for different values of $\bar{\xi}$ [18]. This is the reason why the only results, shown in

Fig. 18, are those obtained with an exponential distribution. As before (Fig. 15), the radiative characteristics $\epsilon'_\lambda(\theta)$ for the optically smooth material are those of 304 L stainless steel for $\lambda = 0.6$ μm, $T = 300$ K, and for $\lambda = 5$ μm and $T = 773$ K; they are shown in Fig. 18 as they correspond to $\bar{\xi} = 0°$. The remarks, made for a single spherical cap (Section 4.1), hold in this

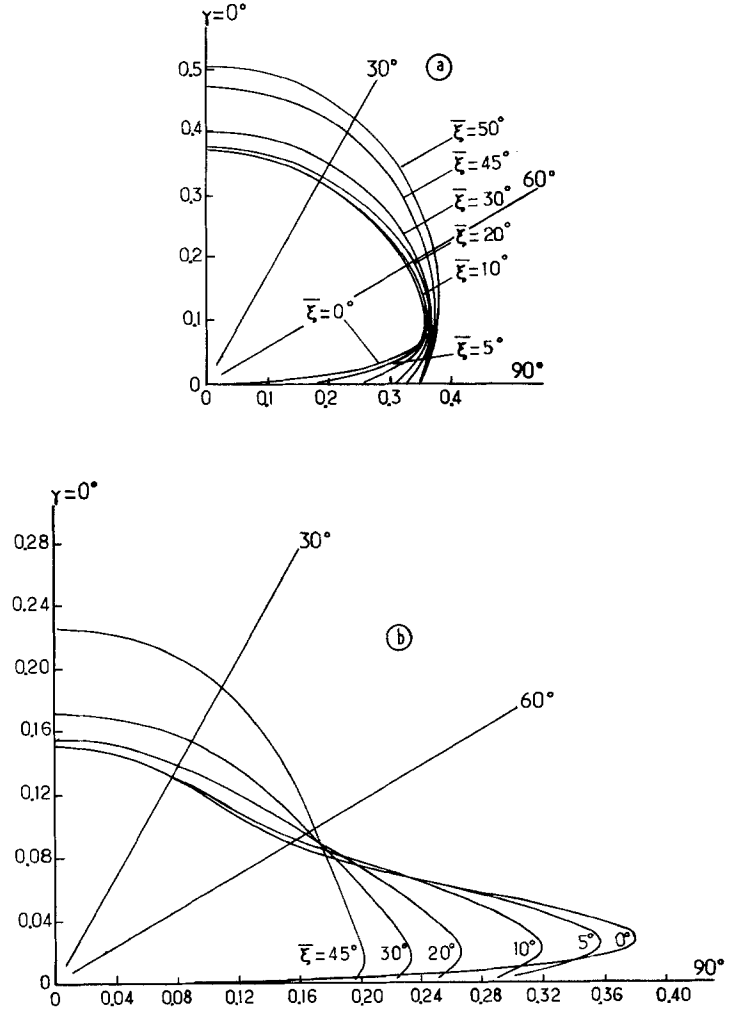

Fig. 18. Directional spectral emissivities $\epsilon'_{\lambda,r}(\gamma)$ calculated with an exponential slope distribution for various values of $\bar{\xi}$. The emissivity $\epsilon'_\lambda(\gamma)$ of optically smooth 304 L stainless steel, represented by the curves $\bar{\xi} = 0°$, corresponds to the following cases: (a) $\lambda = 0.6$ μm, $T = 300$ K; (b) $\lambda = 5$ μm, $T = 773$ K.

case: the emission of the surface is mainly increased towards the normal by the roughness and becomes isotropic, even in the infrared range, for high values of $\bar{\xi}$.

4.3. Comparison of Theoretical Results with Measurements for Ballblasted and Sandblasted Samples

Two experimental arrangements are used to measure the radiative properties of the samples, for the visible and infrared ranges.

For short wavelengths, $0.3 < \lambda < 1$ μm, and for easily reached temperatures, $200 < T < 1000$ K, the emitted fluxes are low so that the directional spectral emissivity cannot be directly measured; however, the measurement of the spectral reflectivities, defined in Section 2, $\rho'^{\frown}_{\lambda}$, Eq. (1a), or $\rho'^{\frown}_{\lambda\,\mathrm{iso.}}$, Eq. (1b), also yields the emissivity, Eq. (2a). An experimental setup, described in refs. [14, 18, 21], uses an integrating sphere, the inner side of which is covered with a barium sulfate layer. Barium sulfate is a good reflector and diffusor, so that the measurement of $\rho'^{\frown}_{\lambda\,\mathrm{iso.}}$ is possible. As in Section 3.2.1, the experiments are conducted under polarized light. A chopped xenon lamp acts as a source so that the emitted continuous flux is eliminated. The precision of the measurements varies from 2 to 5%.

In the infrared range, $2 < \lambda < 15$ μm, and for $500 < T < 1000$ K, the directional spectral emissivities are measured by an experimental arrangement [3, 10] similar to the one described in Section 3.2.1. But, for rough or smooth surfaces, the target area need not be as large as for grooved surfaces. In this case, blackbody and samples of small dimensions are adequate. Finally, the monochromator is replaced by a continuous filter.

Various direct or indirect determinations of the emissivities $\epsilon'_{\lambda r}(\gamma)$ of ballblasted, shotblasted, and sandblasted surfaces were conducted, in the wavelength and temperature ranges indicated above, with a dual purpose:

1. To demonstrate the substantial increase of emission or absorption resulting from superficial treatments easily carried out
2. To compare the experimental results with the values formerly computed

Figure 19a shows the evolution of the quasi-normal spectral emissivity $\epsilon'_{\lambda r}(10°) \simeq \epsilon'_{\lambda r}(0°)$ as a function of the wavelength, with $0.3 < \lambda < 0.8$ μm, for various samples of 304 L stainless steel at room temperature. The increase of emissivity is all the more important as the projectiles, grains or balls, are small; the smaller they are, the deeper they penetrate and the cavity is all the more closed. Measurements of $\epsilon'_{\lambda r}(0°)$ were also done for two samples in the infrared range at 773 K (Fig. 19b). At this temperature, the oxidation [21, 22], as well as the superficial treatment, increases the

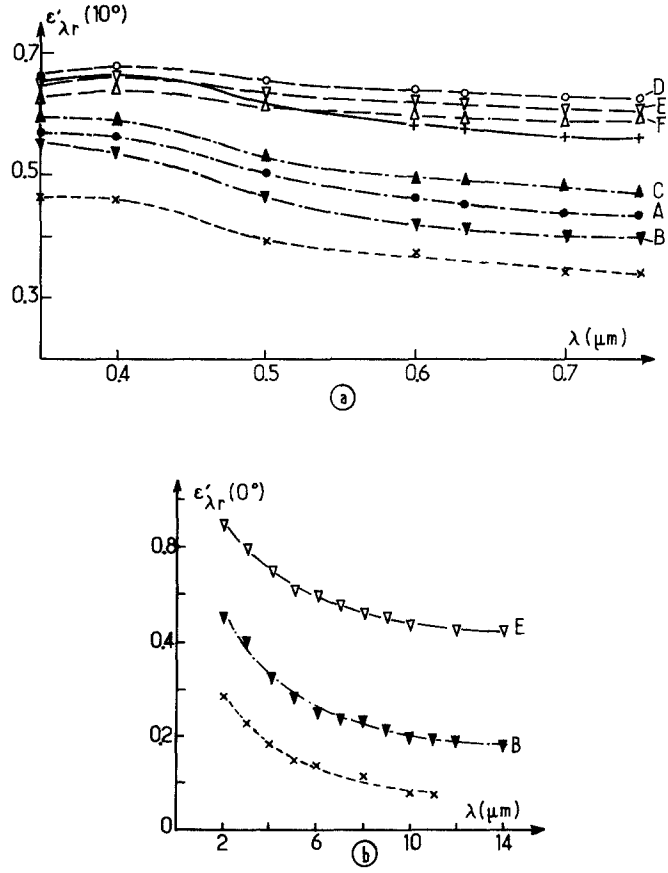

Fig. 19. Directional spectral emissivities of ballblasted and sandblasted 304 L stainless steel samples as a function of the wavelength in the following cases: (a) $\epsilon'_{\lambda r}(10°) \simeq \epsilon'_{\lambda r}(0°)$ for $T = 300$ K; (b) $\epsilon'_{\lambda r}(0°)$ for $T = 773$ K. Curve ×, directional spectral emissivity $\epsilon'_{\lambda}(10°)$ or $\epsilon'_{\lambda}(0°)$ measured for an optically smooth sample. Dot-dashed curves represent samples ballblasted by making use of balls having different mean diameters $\overline{D}$: A, (●), $\overline{D} \simeq 65$ μm; B (▼), $\overline{D} \simeq 150$ μm; C (▲), $\overline{D} = 300$ μm. Long-dashed curves represent samples sandblasted by making use of grains having different mean diameters $\overline{D}$: D (○), $\overline{D} = 35$ μm; E (▽), $\overline{D} \simeq 105$ μm; F (△), $\overline{D} = 590$ μm. Curve +, shotblasted sample.

emissivity, mainly around 2 μm. Generally speaking, sandblasting is the best way to increase the emission; besides the emissivity, $\epsilon'_{\lambda r}$ does not vary very much with the wavelength and the sandblasted surfaces may be considered as grey surfaces.

Figure 20 represents the emissivities of 304 L stainless steel samples for $\lambda = 0.6$ μm and $T = 300$ K, and for $\lambda = 5$ μm and $T = 773$ K. Sample (B)

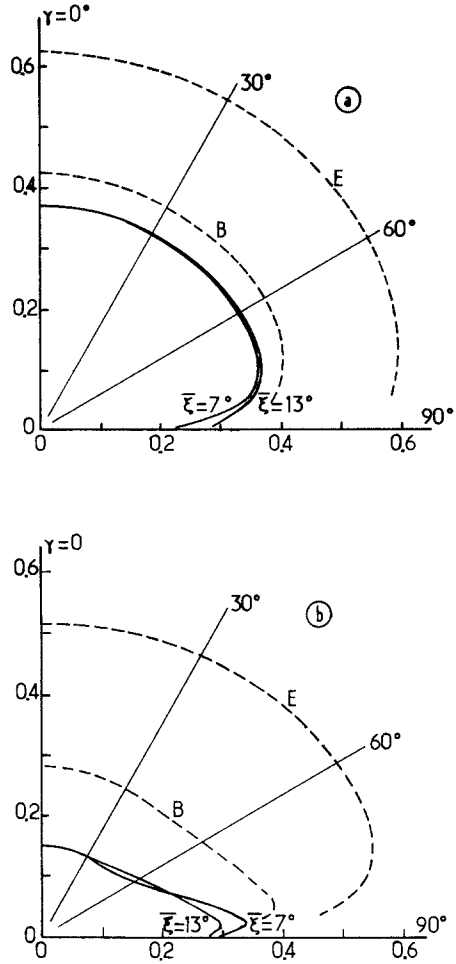

Fig. 20. Comparison between the emissivities $\epsilon'_{\lambda,r}(\gamma)$ measured (dashed curves) and calculated (solid curves) for ballblasted (B) and sandblasted (E) 304 L stainless steel samples in the following cases: (a) $\lambda = 0.6$ μm, T = 300 K; (b) $\lambda = 5$ μm, $T = 773$ K.

was ballblasted with balls of diameters between 105 and 210 μm while sample (E) was sandblasted with white corundum with typical grain diameters of 105 μm. Profile recordings give a quadratic slope average of $\bar{\xi} = 7°$ for the first sample and of $\bar{\xi} = 13°$ for the second sample. The curves of emissivity as a function of γ, computed with these values of $\bar{\xi}$, as shown in Section 4.2 with an exponential slope distribution, are also represented in Fig. 20. It appears that the proposed model is not suited to the type of

roughness created by sandblasting. The same statement can be made for shotblasting. For the ballblasted sample, the agreement between theory and experimental results is rather good in the visible range, though the computed values are small for some reason. However, there is a large discrepancy in the infrared. The measured normal emissivity is twice as large as the calculated one. Moreover, the positions of the maximum of emissivity do not coincide; the maximum is closer to the normal for the experimental curves.

The failure of the proposed model may be understood in the case of sandblasted or shotblasted surfaces; indeed the cavities hollowed out by the grains are deep and distorted so that profile recording is hard to perform and may give erroneous results. Anyway, the real profile might be quite different from that of spherical caps. But the discrepancies observed in the infrared for ballblasted surfaces cannot be interpreted in this way. Some other possible explanations were also discarded after examination, including the following:

1. The spherical caps model, justified *a priori*, may appear questionable. However, computation based upon the $\vee$-groove model [13] with $\bar{\xi} = 7°$ and $\bar{\xi} = 13°$ leads to results almost identical to the ones of Fig. 20b.
2. The measure of the average slope is certainly inaccurate. Anyhow, Fig. 18b proves that no value of $\bar{\xi}$ is adequate to reproduce the experimental data in the infrared. The theory forecasts that $\epsilon'_{\lambda r}(\gamma = 0°)$ is an increasing function of $\bar{\xi}$ whilst $\epsilon'_{\lambda r}(\gamma = 90°)$ is a decreasing function of $\bar{\xi}$, so that the emission becomes almost isotropic; this prediction is contradicted by the experimental results.
3. Both gaussian and exponential distributions, though they are quite different, lead to similar results for $\epsilon'_{\lambda r}(\gamma)$. So the choice of $p(\mu)$ cannot be implicated.

Even if computational methods differ, the theories formerly developed are all based on the same principles and hypotheses. Strangely, they are perfectly suitable for grooves but inadequate for ballblasted surfaces. This behavior suggests two possible explanations.

First, the application of models, based on geometrical optics, is limited to the cases where the average quadratic height σ of the roughnesses is greater than the wavelength λ, that is, $\lambda < \sigma = m\tau/\sqrt{2}$, where τ stands for the length of correlation. This condition is satisfied for the grooved samples of Section 3. But the profile recordings of the ballblasted sample B give a σ value between 4 and 5 μm. Consequently, the inequality $\sigma > \lambda$ is verified for the visible range, where there is a rather good agreement between theory and experiment (Fig. 20a); but it is false in the infrared range, where discrepancies appear (Fig. 20b).

Second, machined with the same tool, the inner sides of a groove are

identical from the radiative point of view to the plane material from which the emissivities $\epsilon'_\lambda(\theta)$ are measured to be included in the computational process. On the contrary, the surface state of the inner sides of the small roughnesses is unknown; it is arbitrarily chosen to be optically smooth. Besides, the physical state is unreliable; the oxidation of the rough samples might be more pronounced than for polished samples at the same temperature. In other words, the curve corresponding to $\bar{\xi} = 0$, on which the computation is based, is unknown.

5. CONCLUSIONS

In some space, nuclear, or solar applications, radiative transfers are the dominant terms of the energy balance. Most of the time, they have to be enhanced through the increase of the emissivity or absorptivity of the chosen material. This can be accomplished by superficial deformations such as grooving or cavity formation, through relatively simple mechanical processes. These treatments present no ageing or adherence problem as paints do.

However, there are some drawbacks to their use. For example, selective materials (or materials called "selective"), which absorb most of the solar flux and are poor radiators, are used for solar energy applications; ϵ'_λ is high in the visible range and low in the infrared one. Superficial deformations reduce the selectivity of materials since the cavity effect is all the more important as the material spectral emissivity is low. Anyhow, selectivity is not always useful. Moreover, cavity effect is a relative value, and an important relative rise of the emitted flux, for example, may be tolerated if its absolute value is lower than the concomitant increase of the absorbed flux. In particular, for a high concentration solar receiver, the critical factor is the solar absorptivity, which has to be increased whatever emissivity may be.

The influence of superficial deformations or roughness can be determined through experiments or calculations. Two cases were presented in this paper.

1. For variously shaped grooves, the characteristic dimension σ is large compared to the wavelength λ; various theories, based on the concepts of geometrical optics, give results in good agreement with the experimental data. This is true if the real directional spectral properties of the inner sides of the grooves, previously measured from a plane sample, are taken into account. Relatively small discrepancies are recorded and are probably due to a misunderstanding of the precise reflection law, which is certainly not perfectly isotropic nor specular.

2. When the characteristic dimension σ is close to λ, a clear discrepancy appears between the measured and calculated results. This happens

even if the cavity shape is correctly represented (as, for example, spherical caps for ballblasted surfaces) and especially in the infrared range where λ is almost equal to σ. The discrepancy can't be ascribed merely to the invalidity of geometrical optics. Inner sides of the cavities are surely not optically smooth as we have assumed; their radiative behavior is unobservable. Anyhow, differences between theoretical and experimental results are too important to be ascribed to the two reasons presented.

In conclusion, theories have to be improved in order to explain the radiative properties of rough surfaces when the dimensions of the cavities are close to the wavelength λ. It is interesting to observe that the measured emissivities are always greater than those calculated from any of the proposed models. This observation stands for models based on geometrical optics as well as for the models based on physical optics.

ACKNOWLEDGMENTS

The authors wish to thank J. M. Ané and J. F. Sacadura for their important participation in the work presented in this paper.

REFERENCES

1. R. Siegel and J. R. Howell, *Thermal Radiation Heat Transfer* (McGraw-Hill, New York, 1972).
2. M. Huetz-Aubert and J. Taine, *Rev. Gén. Therm.*, **17**:755 (1978).
3. P. Demont, M. Huetz-Aubert, and J. F. Sacadura, *Rev. Phys. Appl.* **17**:239 (1982).
4. E. M. Sparrow and S. H. Lin, *Int. J. Heat Mass Transfer* **5**:1111 (1962).
5. R. B. Zipin, *J. Res. Nat. Bur. Stand.* **70C**:275 (1966).
6. W. Z. Black and R. J. Schoenhal, *J. Heat Transfer, Trans. ASME Serie C* **90**:420 (1968).
7. E. M. Sparrow and V. K. Jonsson, *J. Appl. Mech.* **E30**:237 (1963).
8. E. M. Sparrow, *J. Heat Transfer, Trans. ASME Serie C* **84**:283 (1962).
9. P. Druelle and M. Huetz-Aubert, VIth Int. Heat Transfer Conf., Toronto, Canada, 1978.
10. H. Tran N'Guyen, Thèse Docteur Ingénieur, Ecole Centrale des Arts et Manufactures, Paris (June 1981).
11. E. M. Sparrow, *J. Heat Transfer, Trans. ASME Serie C* **82**:375 (1960).
12. P. Druelle, Thèse Docteur Ingénieur, Ecole Centrale des Arts et Manufactures, Paris (October 1978).
13. J. F. Sacadura, Thèse Doctorat d'Etat, Lyon I (July 1980).
14. M. Huetz-Aubert and J. F. Sacadura, *Rev. Phys. Appl.* **17**:251 (1982).
15. F. Abeles, Int. Conf. Materials for Photothermal Solar Energy Conversion, Corsica, France, 1980; *J. Phys.* **42**:C1-33 (1981).
16. R. C. Birkebak and A. Abkulkadir, *Int. J. Heat Mass Transfer* **19**:1039 (1976).
17. J. C. Godon, Thèse 3ème cycle, Paris VI (1977).
18. P. Demont, Thèse Docteur Ingénieur, Ecole Centrale des Arts et Manufactures, Paris (November 1980).
19. P. Demont, M. Huetz-Aubert, and H. Tran N'Guyen, Symp. Int. Systèmes de Conversion thermodynamique de l'Energie solaire, Marseille, France, 1980.
20. P. Beckmann and A. Spizzichino, *The Scattering of Electromagnetic Waves* (Pergamon Press, Elmsford, N.Y., 1963).
21. P. Demont, H. Tran N'Guyen, and J. F. Sacadura, Int. Conf. Materials for Photothermal Solar Energy Conversion, Corsica, France, 1980; *J. Phys.* **42**:C1-161 (1981).
22. J. M. Ané, J. F. Sacadura, and P. Stekelorom, VIIth Int. Heat Transfer Conf., Munich, Germany, 1982.